Available online at www.sciencedirect.com
ScienceDirect
Journal of Catalysis 248 (2007) 165–174
JOURNAL OF CATALYSIS
www.elsevier.com/locate/jcat

Preparation of silica- and carbon-supported cobalt by electrostatic adsorption of Co(III) hexaammines

L. D'Souza [a], L. Jiao [a], J.R. Regalbuto [a,*], J.T. Miller [b], A.J. Kropf [c]

[a] *Department of Chemical Engineering, University of Illinois, MC 110 810 S Clinton Street, Chicago, IL 60607 7000, USA*
[b] *BP Research Center, E-1F, 15l0 W Warrenville Road, Naperville, IL 60563, USA*
[c] *Argonne National Laboratory, Chemical Engineering Division, Argonne, IL 60439, USA*

Received 15 December 2006; revised 7 March 2007; accepted 11 March 2007

Available online 23 April 2007

Abstract

Application of the simple, rational catalyst synthesis method of strong electrostatic adsorption was applied to hexaammine cobalt(III) chloride (CoHA) complexes over silica and carbon, which potentially affects the preparation of Fisher–Tropsch and other catalysts. Uptake versus pH was studied, and resulting materials were characterized by powder XRD, EXAFS, XANES, and STEM at each stage of the preparation procedure. Large differences occurred when CoHA was contacted at high pH over silica and carbon surfaces with similar points of zero charge. The Co ammine–silica interaction could be described by a purely electrostatic interaction, was very strong, and prevented reduction up to the high temperatures at which significant Co sintering occurred. However, sufficient interaction existed so that the normally lower-temperature stable hexagonal close-packing phase was retained by the metal crystallites on silica. Over carbon, CoHA underwent a reductive deammination on contact with the carbon to form large crystals of Co_3O_4. While this precursor phase reduces at much lower temperature than the silica-supported Co ammines, the large initial size of the Co_3O_4 phase also prevented the formation of small Co particles. Our findings demonstrate that high Co metal dispersion on carbon might be achieved with synthesis parameters (i.e., other Co complexes, carbons, or impregnation conditions) that yield a highly dispersed Co precursor.

Keywords: $[Co(NH_3)_6]Cl_3$; Co_3O_4; Co/SiO_2; Co/C; Co EXAFS; STEM; Fisher–Tropsch synthesis

1. Introduction

In an effort to help "turn the art of catalyst preparation into science," we have developed the method of strong electrostatic adsorption (SEA) as a simple, rational approach to synthesizing highly dispersed metals on oxide and carbon supports [1,2]. The SEA method is based on an electrostatic mechanism in which the functional groups (typically hydroxyl) on the support surface can be protonated and deprotonated and thus positively or negatively charged as a function of pH (relative to the point of zero charge [PZC]). At the pH of strongest interaction, oppositely charged metal coordination complexes adsorb in a well-dispersed monolayers; in many cases, the high dispersion of the precursor phase can be retained as the precursor is reduced to metal [1–3].

To date, the electrostatic mechanism has been demonstrated mainly for noble metal complexes, including anionic Pt chlorides (and related hydrolysis complexes) over alumina [4,5], cationic Pt tetraammines over silica [3,6], and both over carbon [7]. Recently, electrostatic adsorption was suggested as the reason for Pt and Cu overexchange in low Al zeolites [8].

In the current work, the extension of SEA is made to an important base metal, cobalt. Supported Co catalysts have potentially high activity and selectivity for a number of reactions, including water–gas shift (WGS) [9–11], steam reforming of ethanol [12], Fischer–Tropsch [13,14] and methylamine [15] synthesis, and cyclocarbonylation of acetylenes [16]. Cobalt catalysts have also found application due to their sulfur resistance [17,18]. Mixed cobalt-oxide catalysts have also been widely used for the WGS reaction [17,19,20].

* Corresponding author. Fax: +1 312 996 0808.
E-mail address: jrr@uic.edu (J.R. Regalbuto).

0021-9517/$ – see front matter
doi:10.1016/j.jcat.2007.03.010

A commonly available cobalt complex is cobalt(III) hexaammine ($[(NH_3)_6Co]^{3+}$ or CoHA). This should be strongly adsorbed at high pH over low-PZC materials, such as silica or oxidized carbon. Silica is commonly used as a support material for Co because of its high surface area [21] and also is often used as a (oxide) support for comparison with carbon. Recently, carbon was cited as a good candidate for FT synthesis, because lower Co–support interactions relative to silica lead to lower reduction temperature and better Co dispersion [22]. Well-dispersed cobalt oxide on carbon is also a potential intermediate in the fabrication of Pt–Co bimetallic fuel cell electrocatalysts [23].

Table 1 details some of the important literature reports on Co/C and Co/SiO_2 preparations. The majority of the researchers have used $Co(NO_3)_2$ as cobalt precursor, and with this complex and the common preparation of dry impregnation, and at high Co loadings the resulting particle sizes are often relatively large. Cobalt crystallite size appears to be a strong function of metal loading, independent of preparation method [24,31]. The "ammonia method" [24] yields smaller particle sizes relative to other preparations through a proposed chemical interaction involving phyllosilicate phases formed from intermediate Co(II) aquo-ammine ($[Co(H_2O)_{6-n}(NH_3)_n]^{2+}$) complexes.

In a systematic series of preparations over carbon nanofibers [31], the smallest particle sizes were achieved at the lowest loadings, irrespective of whether dry impregnation or ion adsorption was used. Reasonably high dispersion (7.8 nm particles) of Co on carbon at high Co loading was achieved with homogeneous deposition–precipitation with ammonia evaporation [22]. Perhaps the best success at high Co dispersion with narrow particle size distribution has been found for a sol–gel preparation with silica [24]. The current effort is directed at high Co dispersions with a simple, single-step impregnation process.

Toward this end, Co(III) ammine uptake and the dispersion of the reduced Co phase were compared over a silica and an oxidized carbon of approximately the same PZC. At each step of the preparation, the Co species are characterized by XRD, EXAFS, XANES, and STEM. A dramatic difference in the interaction of CoHA with the respective surfaces was revealed; whereas CoHA uptake on silica appears to be completely electrostatic and the Co ammines strongly interact with the silica surface, the adsorption appears to have a reactive component over the carbon. CoHA contacted with the high-surface area graphite reacted spontaneously to yield Co_3O_4 at room temperature and pressure.

2. Experimental

In preliminary studies, cobalt(III) hexaammine (CoHA) was seen to be much more soluble than Co(II) hexaammine over the wide range of pH used in this study, and so was chosen as the Co precursor. It, metallic Co, CoO, and Co_3O_4 were obtained from Aldrich. High-surface area carbon (TIMREX HSAG 300, 291 m^2/g) was obtained from TIMCAL Graphite and Carbon. Silica Vn-3s was obtained from Degussa. The N_2 BET surface area and pore volume were 175 m^2 g and 1.0 cc g, respectively, and were not affected by any of the catalyst preparation steps. The PZC was 4.0 for both silica and graphite.

The equilibrium adsorption uptake of CoHA onto silica and carbon was determined as a function of pH from solutions of constant metal concentration. Adsorption experiments were conducted with an excess of liquid to prevent large shifts in the solution pH due to the oxide buffering effect [25]. The surface loading indicates the amount of support surface per liter of impregnation solution. For example, 0.1 g of 250 m^2/g silica in 50 ml of solution yields a surface loading of 500 m^2/L, or about a 500-fold excess of the pore volume. The 50-ml polypropylene bottles containing 200 ppm CoHA solutions and support were shaken for 1 h, after which 3–4 ml of filtered solution was analyzed for Co by ICP. The cobalt uptake was determined as the difference in Co concentrations in the precontacted and post-

Table 1
Literature survey of preparation methods for Co/C and Co/SiO_2 catalysts

Reference	Precursor	Wt%	Particle size (nm)	Method	Pretreatment	Remarks
				Amorphous SiO_2		
[24]	$Co(NO_3)_2$	3–46	3.8–16	Ammonia	650 °C reduction	
[21]	$Co(NO_3)_2$	15	1.9–7.9	Dry impregnation	500 °C calcination, 450 °C reduction	
[46]	$Co(NO_3)_2$	25	20–35	Sol–gel	Calcination	
[47]	$Co(NO_3)_2$	20	3–5	Sol–gel	550 °C calcination, 500 °C reduction	
[47]	$Co(NO_3)_2$	20	26	Dry impregnation	550 °C calcination, 500 °C reduction	
[42]	$Co(NO_3)_2$	2–20	12–38	Dry impregnation	450 °C calcination, 400 °C reduction	hcp + fcc, fcc is predominant
[45]	Co	2.3×10^{17} Co/cm^2	5	Ion implantation		hcp-to-fcc occurred at 800 °C
[22]	$Co(CO_3)$	15	13	HDP w/NH_3 evaporation	500 °C reduction	fcc, hcp, CoO
				Carbon		
[22]	$Co(CO_3)$	15	7.9	HDP w/NH_3 evaporation	350 °C reduction	fcc, CoO
[48]	$Co(NO_3)_2$	9.5	12	Dry impregnation	350 °C reduction, *RT* O_2 passivation	fcc, CoO
[49]	$Co(NO_3)_2$	3	–	Evaporative deposition		
[40]	$Co(NO_3)_2$	11	27	HDP w/urea	120 °C drying, 350 °C reduction	
[40]	$Co(CO_3)$	9.0	12.8	HDP w/NH_3	–	
[40]	$Co(NO_3)_2$	9.9–22	9.8–16	Water, dry impregnation	–	
[40]	$Co(NO_3)_2$	1.1–7.5	4.5–5.9	EtOH, dry impregnation	–	
[40]	$Co(CH_3COO)_2$	1.0–4.2	2.6–4.1	Water, dry impregnation	–	
[40]	$Co(CO_3)$	0.8	3.0	Ion ads., w/NH_3	–	

contacted solutions. The pH was adjusted with 0.1 M HNO_3 and 0.1 M NaOH.

After the amount of CoHA adsorbed at each pH was determined, larger (2 g) samples of catalysts were prepared at the pH of maximum uptake, which corresponds to optimal condition for strong electrostatic adsorption. The filtered solids were air-dried overnight and calcined at various temperatures in a muffle. Reduction was performed in a fixed-bed tubular reactor at 320 °C with 100% flowing H_2, or with 4% H_2 (balance He) at Argonne in the in situ XAFS cell. Representative samples reduced with 100 and 4% H_2 showed no difference.

XRD analyses were performed using a Siemens D5000 diffractometer with Cu$K\alpha$ radiation ($\lambda = 1.5406$ Å) operated at 30 kV and 40 mA, operating in Bragg–Brentano geometry. A "locked coupled" scan mode in the 20°–70° 2θ range, step size of 0.01°, and 2.5 s exposure in each point were used.

TEM of the catalysts were obtained by adding isopropanol and sonicating this slurry for 5 min. Then the samples were placed onto a carbon-coated copper grid. STEM and EDX experiments were done using a JEOL electron microscope (JEM-2010F FasTEMm FEI) operated at 200 kV and extracting voltage of 4500 V. The copper grid (200 mesh, CuPK/100) was supplied by SPI Supplies. Approximately 200 particles were considered for size distribution calculation.

EXAFS measurements were performed at the Advanced Photon Source (APS) at Argonne National Laboratory (Argonne, IL) on the undulator beamline of the Materials Research Collaborative Access Team (MRCAT). Details of the EXAFS data collection and analysis have been given previously [26], the only difference here being that the data were collected purely in transmission. Most of the powdered solid samples were pressed into thin disks. The data fitting was done with the software WinXAS 97, version 1.0. Pure $[Co(NH_3)_6]Cl_3$, Co foil, CoO, and Co_3O_4 were used as XANES standards. CoHA and Co foil were used as Co–N ($N_{Co–N} = 6$, $R = 1.97$ Å) and Co–Co ($N_{Co–Co} = 12$, $R = 2.55$ Å) EXAFS references, respectively. The results were generally accurate to ±10% in coordination number. The first shell fits were done in R-space of the k^2-weighted data from 2.7 to 12.2 $Å^{-1}$.

3. Results

Results from the metal adsorption experiments include both pH shifts and metal uptake. First, pH shifts for both carbon and SiO_2 are given in Fig. 1A and are compared to the shifts seen with no metal in solution. The PZC of pure silica and carbon are both about 4.0 (seen as the plateaus in the plot [6,27]). After 1 h of adsorption, the pH plateau is relatively unchanged for silica, whereas for carbon, the plateau has increased to about 9, close to the PZC of pure Co_3O_4. The uptake of CoHA on SiO_2 and carbon is shown in Fig. 1B. The maximum CoHA uptake was found to be 1.6 μmol/m^2 on SiO_2 and 3.5 μmol/m^2 on carbon at pH 13. These values amount to nearly 1.7 wt% Co/SiO_2 (25% yield) and 6 wt% of Co/C (93% yield). Measurements beyond pH 13 were not done, because it was presumed that uptake beyond pH 13 will be decreased as ionic strength increases dramatically [6]. Thus, the optimum pH for adsorption is taken as approximately 11.5. The pH and CoHA uptake were unchanged from 1 to 24 h for SiO_2 and changed only slightly for carbon. (Co/C is discussed in more detail elsewhere [28].)

Larger quantities of Co/SiO_2 and Co/C (3.5 μmol/m^2 or 6.0 wt% Co on carbon, 1.6 μmol/m^2 or 1.7 wt% on SiO_2) were prepared for further characterization by powder XRD, XAS, and STEM. Powder XRD results of dried, calcined, and reduced (pure) CoHA, Co/C, and Co/SiO_2 are given in Fig. 2.

Reduction of pure CoHA in flowing hydrogen at 300 °C leads to partial reduction of Co^{3+} to Co^{2+} with formation of $CoCl_2{\cdot}2H_2O$ (Fig. 2IB), which is in accordance with Khalil and Mousssa's observation [29] (PDF no. 25-0242; major peaks at $2\theta = 20.8°$, 31.42°, 33.1°, 37.9°, 42.3°, 46.6°, and 58.1°). The source of chloride for $CoCl_2{\cdot}2H_2O$ formation is from counterions on CoHA. An increase of reduction temperature to 650 °C results in the formation of two metallic phases (Fig. 2ID), with sharper, more intense peaks at $2\theta = 44.21°$ and 51.2° corresponding to a relatively sintered fcc phase and broader, lower-intensity peaks at $2\theta = 41.7°$, 44.8°, 47.6°, and 62.7°, representative of smaller hcp particles. Calcination 450 °C partially reduces CoHA to the stable spinel oxide, Co_3O_4 (Fig. 2IC)

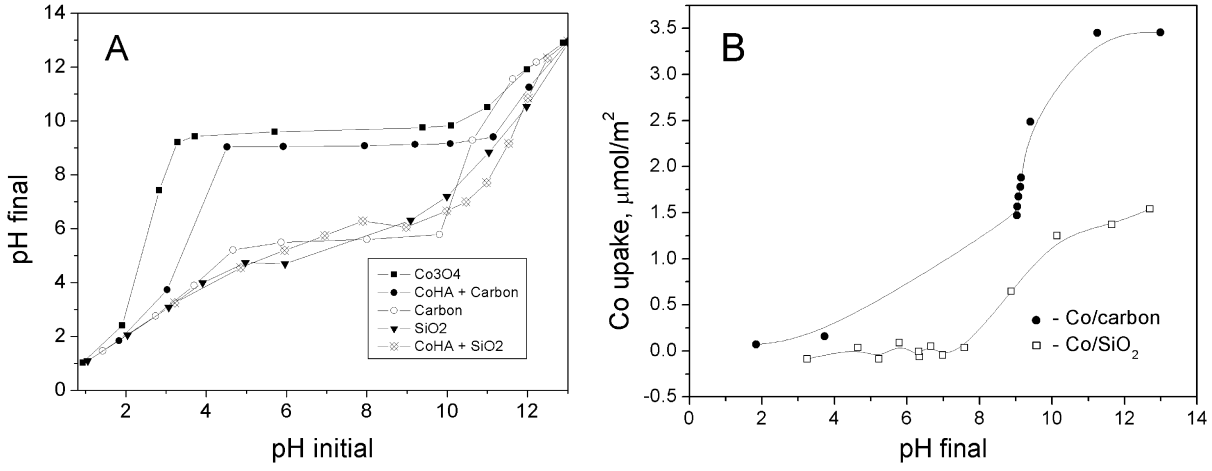

Fig. 1. Co adsorption measurements (200 ppm Co, 1000 m^2/L), (A) solution pH shifts with CoHA + SiO_2, and CoHA + carbon; control experiments for carbon, SiO_2, and Co_3O_4 systems have also been given; (B) CoHA uptake on SiO_2 and carbon versus pH.

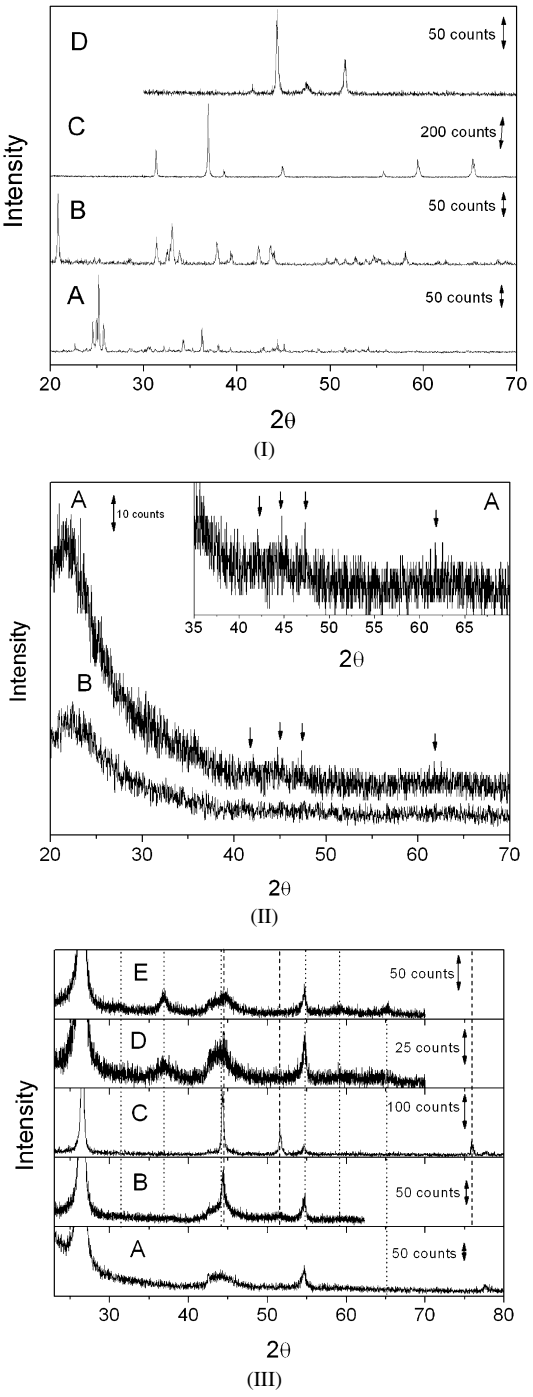

Fig. 2. Powder X-ray diffraction patterns of I—(A) pure CoHA, (B) CoHA reduced at 300 °C, (C) CoHA calcined at 450 °C, and (D) pure CoHA reduced in 100% H_2 at 650 °C; II—(A) CoHA/SiO_2 reduced at 650 °C and (B) CoHA/SiO_2 calcined at 450 °C (inset: enlarged portion of A); III—(A) carbon support, (B) CoHA/C reduced at 500 °C, (C) CoHA/C reduced at 650 °C, (D) CoHA/C dried at room temperature, and (E) CoHA/C calcined at 450 °C.

(PDF no. 74-1657; major peaks at $2\theta = 31.3°$, 36.9°, 38.6°, 44.9°, 55.7°, 59.4°, and 65.3°).

The color of CoHA/SiO_2 dried at room temperature was light orange, but changed to dark sky blue when calcined at 100 °C and light sky blue when calcined at higher temperature. That color was preserved even after calcination at 800 °C. No XRD peaks were observed after calcination of CoHA/SiO_2 up to 800 °C; a typical spectrum of the catalyst calcined at 450 °C is shown in Fig. 2IIB. Both calcined and dried materials were stable to reduction in flowing hydrogen up to 600 °C, but one that reduced at 650 °C showed low-intensity, broad peaks of metallic hcp Co (Fig. 2IIA) at $2\theta = 41.7°$, 44.8°, 47.6°, and 62.7° (PDF no. 05-0727), which are indicated by arrows.

Powder XRD spectra for CoHA/carbon dried at room temperature and calcined at 450 °C are shown in Fig. 2III. The pure carbon pattern is shown in Fig. 2IIIA; diffraction peaks are at $2\theta = 26.6°$, 44.7°, 43.7°, 44.7°, and 54.7° (PDF no. 26-1076). Peaks at $2\theta = 31.3°$, 36.9°, 38.6°, 44.9°, 55.7°, 59.4°, and 65.3° (dotted lines) for the sample impregnated and dried at room temperature (Fig. 2IIID) indicate that Co_3O_4 forms immediately on contact of CoHA with the graphite surface. After calcination at 450 °C, the peaks sharpen, indicating sintering of Co_3O_4 (Fig. 2IIIE). Fig. 2IIIB and C gives the diffraction pattern of Co/C reduced at 500 and 650 °C, respectively, it is obvious from diffraction pattern that peaks due to Co_3O_4 have vanished and peaks due to Co fcc metal at $2\theta = 44.21°$, 51.2°, and 75.85° (PDF no. 15-0806; dashed lines) have appeared. The peak at 44.2° superimposes that of C at the about the same position.

Generally, pure cobalt undergoes the hcp-to-fcc phase transition around 400 °C [30], but it is interesting to note that cobalt Co/SiO_2 has hcp crystals even after the reduction at 650 °C. One reason may be due to formation of cobalt metal directly from the ammine precursor. In the case of Co/C, the formation of cobalt metal is from cobalt(II, III) oxide and yields the fcc phase of cobalt.

To better characterize the Co species during preparation, EXAFS measurements were obtained after various pretreatments. Fig. 3 shows the k^2-weighted magnitude of the Fourier transform of the reference compounds [CoHA, Co(II) oxide (CoO), Co(II, III) oxide (Co_3O_4), and Co foil]. The first shell fits are given in Table 2. CoHA (Fig. 3Ia) has 6 Co–N bonds at 1.97 Å (peak at about 1.5 Å in the uncorrected FT). Reduction of CoHA at 320 °C, gives a peak at higher R, which, from the phase and bond distance, is consistent with 4 Co–Cl bonds at 2.41 Å (Fig. 3Ib) and is in agreement with powder XRD results for the $CoCl_2$ phase. The magnitude of the Fourier transform for pure CoO (Fig. 3IIa) has a peak at about 1.5 Å due to 6 Co–O at 2.14 Å and a higher shell peak (2.5 Å) due to scattering from Co atoms (i.e., binding Co–O–Co atoms). CoO is partially reduced by H_2 at 320 °C (Fig. 3IIb) to Co metal with a $N_{Co–Co} = 6.1$ at a distance of 2.55 Å. A fit of the XANES spectra indicates that about 50% of the Co is metallic with 50% unreduced CoO. Because only a portion of the Co is reduced, the true coordination number is given by the fit value divided by the fraction of metallic Co (e.g., $6.1/0.5 = 12.2$), indicating formation of large metallic Co particles. Perhaps slow transport of hydrogen in the large-grained of CoO was the reason for its incomplete reduction. The Fourier transform for Co_3O_4 also has peaks for Co–O and higher shells for scattering from bridging Co–O–Co. In Co_3O_4, half of the Co–O bonds were tetrahedrally coordinated (at 1.92 Å) and half were octahedrally coordinated (1.94 Å). The Co–O first shell fits of 5 Co–O at 1.94 Å is in good agreement with the XRD structure.

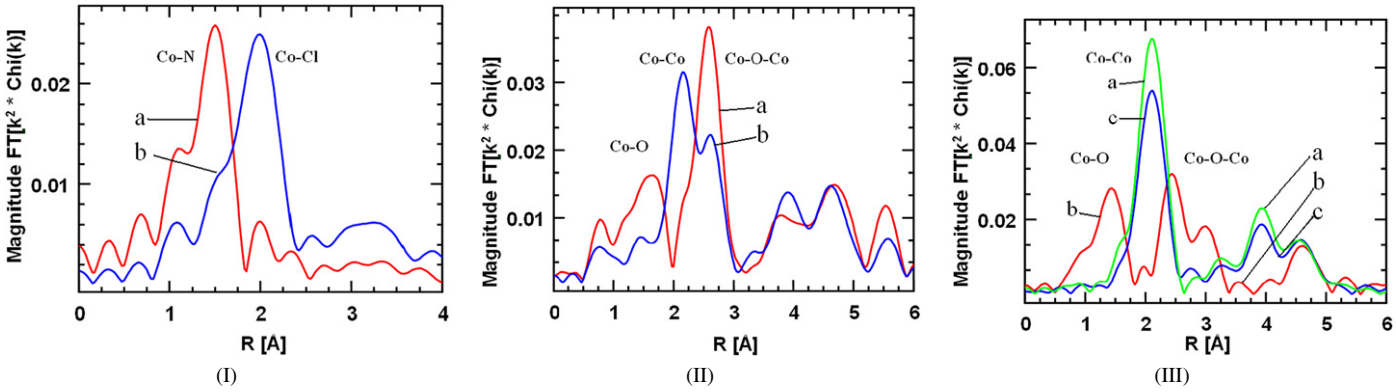

Fig. 3. EXAFS analysis of reduction of different cobalt species: (I) (a) pure CoHA, (b) CoHA reduced at 320 °C; (II) (a) pure CoO, (b) CoO reduced at 320 °C; and (III) (a) Co foil, (b) pure Co_3O_4, (c) Co_3O_4 reduced at 320 °C.

Table 2
Co EXAFS fits for reference compounds (k^2: $\Delta k = 2.75-12.2^{-1}$ Å)

Compound	Treatment	Backscatter	CN	R (Å)	DWF ($\times 10^3$)	E_0 (eV)
$Co(NH_3)_6Cl_3$ (CoHA)	None-mixed with SiO_2	Co–N	6.0	1.97	0.7	0.3
CoHA reduced	H_2 at 320 °C	Co–Cl	4.0	2.41	6.0	−1.0
CoO	None-mixed with SiO_2	Co–O	6.0	2.14	4.3	−0.5
CoO reduced	H_2 at 320 °C	Co–O	2.0	2.14	−0.3	1.4
		Co–Co	6.1	2.55	0.5	4.5
Co_3O_4	None-mixed with SiO_2	Co–O	5.0	1.94	−3.0	−4.1
Co_3O_4 reduced	H_2 at 320 °C	Co–Co	10.1	2.51	0.5	−0.6
	Pre-reduced (reduced, *RT* oxidized, and re-reduced)					
Co_3O_4 reduced 400 °C	4% H_2 at 300 °C	Co–Co	4.6	2.50	0.5	7.7
Co_3O_4 reduced 400 °C	100% H_2 at 300 °C	Co–Co	4.6	2.51	0.5	8.4

At 320 °C, Co_3O_4 is fully reduced to metallic Co (Fig. 3IIIc), with a $N_{Co-Co} = 10.1$ at 2.51 Å. The coordination number is consistent with moderately sized metallic particles of 50–100 Å [31].

The k^2-weighted magnitude of the Fourier transform spectra of CoHA adsorbed and calcined on SiO_2 are compared in Fig. 4. The first shell fits are given in Table 3. Adsorption of CoHA onto silica and dried at room temperature was identical to that of pure CoHA, that is, $N_{Co-N} = 6$ at 1.95 Å. After calcination at 100 °C, the number of Co–N bonds decreased to 4 with no change in the bond distance. Calcination at temperatures up to 450 °C (Fig. 4d) indicate no further change in the state of Co. The change in the coordination number from 6 to 4 and the change in the edge position from 7.721 to 7.715 eV (Fig. 5) are consistent with reduction of Co^{3+} to Co^{2+}, that is, adsorbed Co(II) tetraammine.

Unlike CoHA adsorbed on silica, CoHA undergoes structural transformation on adsorption onto graphite (Fig. 6). The first shell fits are given in Table 4, and the fit of the Co–O peak ($N_{Co-N} = 4.7$ at 1.93 Å) and the position of the Co–O–Co peak suggest that Co_3O_4 is formed at room temperature. The size of the Co–O–Co peaks (from about 2.0 to 3.2 Å) of CoHA/C dried at room temperature or 100 °C suggests smaller Co_3O_4 particles, which sinter on calcination at 200 °C. The EXAFS confirms the XRD (Fig. 2) that Co(III) hexaammine transforms to Co_3O_4 on adsorption onto graphite and that sintering occurs on high-temperature calcination.

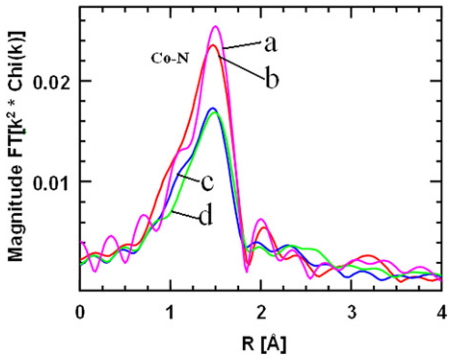

Fig. 4. EXAFS analysis of effect of adsorption/calcination on CoHA/SiO_2: (a) pure CoHA ($N_{Co-N} = 6.0$), (b) CoHA/SiO_2 dried at room temperature ($N_{Co-N} = 6.0$), (c) CoHA/SiO_2 dried at 100 °C ($N_{Co-N} = 4.2$), and (d) CoHA/SiO_2 calcined at 450 °C ($N_{Co-N} = 4.2$).

The reduction of CoHA on silica and graphite supports is shown in Fig. 7. Reduction of CoHA on silica by H_2 at 320 °C and calcination of CoHA on silica at 450 °C lead to a decrease in the number of Co–N bonds to 4 (Table 3). Similar results obtained for the sample calcined at 450 °C followed by reduction at 320 °C; in other words, the calcined sample's chemical state did not change further due to reduction at 320 °C.

In addition, there was a shift in the edge energy consistent with a reduction of Co^{3+} to Co^{2+} (Fig. 5 a and c). CoHA on silica is easily reduced to cobalt(II) tetraammine by heating in air or H_2 above 100 °C; however, the ammine ligands are not eas-

Table 3
Co EXAFS fits for $Co(NH_3)_6^{3-}$ on silica (k^2: $\Delta k = 2.75-12.2^{-1}$ Å)

Catalyst	Treatment	Backscatter	CN	R (Å)	DWF ($\times 10^3$)	E_0 (eV)
CoHA–SiO_2	Dried *RT*	Co–N	6.0	1.95	0.7	−2.1
CoHA–SiO_2 reduced[1]	H_2 at 320 °C	Co–N	4.2	1.98	0.7	0.3
CoHA–SiO_2 100 °C cal[1]	Dried 100 °C	Co–N	4.2	1.96	0.7	−2.1
CoHA–SiO_2 300 °C cal[1]	Calcined 300 °C	Co–N	4.4	1.97	0.7	−1.6
CoHA–SiO_2 450 °C cal[1]	Calcined 450 °C	Co–N	4.2	1.98	0.7	−0.6
CoHA–SiO_2 450 °C cal[1]	Calcined 450 °C C, H_2 at 320 °C	Co–N	4.3	1.98	0.7	0.2

[1] Edge position consistent with Co^{2+}.

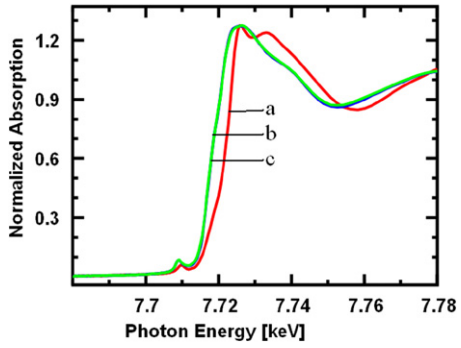

Fig. 5. Co *K*-edge XANES for $Co(NH_3)_6^{3+}$ on silica (7.68–7.78 keV): (a) CoHA dried at *RT*, (b) CoHA calcined at 500 °C, and (c) CoHA reduced at 320 °C.

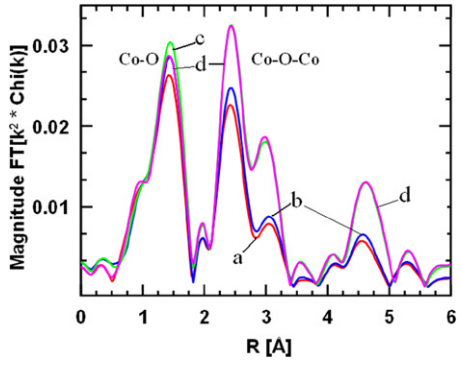

Fig. 6. EXAFS analysis of effect of adsorption/calcination on CoHA/C: (a) room temperature dried ($N_{Co-N} = 4.7$ and $R = 1.93$ Å), (b) 100 °C calcined ($N_{Co-N} = 4.8$ and $R = 1.93$ Å), (c) 200 °C calcined ($N_{Co-N} = 5.2$ and $R = 1.92$ Å), and (d) pure Co_3O_4 ($N_{Co-N} = 5$ and $R = 1.94$ Å).

ily oxidized or Co^{2+} reduced in the silica-adsorbed cobalt(II) tetraammine.

Wheres CoHA on silica was resistant to reduction to metallic Co, reduction of CoHA on graphite (i.e., supported Co_3O_4 nanoparticles) was partially reduced to metallic Co at 320 °C in H_2 (Table 4; Fig. 7d). In addition, the fit of the Co–O indicated a change in the CoO bond distance to 2.13 Å, characteristic of CoO rather than Co_3O_4 ($R = 1.94$ Å). Furthermore, the higher shell peaks were similar to those of CoO. The XANES spectra were fit with a linear combination of CoO and Co foil. The fraction of metallic Co on CoHA/C dried at room temperature was 0.5, and the fraction of metallic Co decreased to 0.3 for CoHA/C calcined at 200 °C. For both samples, Co_3O_4 reduced to CoO before reduction to metallic Co, and the larger (CoO) particles were more difficult to reduce.

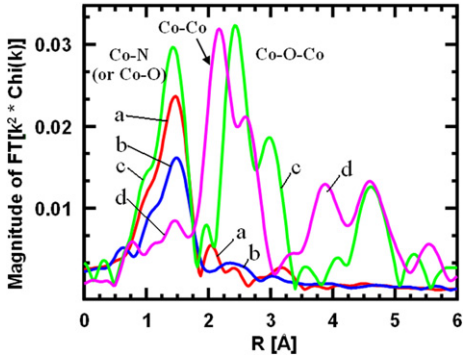

Fig. 7. Effect of reduction at 320 °C on $Co(NH_3)_6^{3+}$ on silica and carbon supports: (a) CoHA on silica dried at 100 °C ($N_{Co-N} = 4.2$, $R = 1.98$ Å), (b) CoHA on silica calcined at 450 °C ($N_{Co-N} = 4.3$, $R = 1.98$ Å), (c) CoHA on carbon dried at 25 °C ($N_{Co-O} = 2.2$, $R = 2.13$ Å; $N_{Co-Co} = 6.6$, $R = 2.51$ Å; $N_{Co-Co(O)Co} = 5.8$, $R = 3.02$ Å), and (d) CoHA on carbon calcined at 200 °C ($N_{Co-O} = 2.7$, $R = 2.12$ Å; $N_{Co-Co} = 4.8$, $R = 2.51$ Å; $N_{Co-Co(O)Co} = 8.8$, $R = 3.02$ Å—typical of CoO).

Bright-field transmission electron micrographs for CoHA/SiO_2 calcined at 450 °C are shown in Fig. 8a. There are no apparent particles, implying that the CoHA is molecularly adsorbed. Those of CoHA/silica reduced at 650 °C in H_2, for which XRD (Fig. 2) indicated small, metallic particles, is shown in Fig. 8b. The average particle size was 6.0 ± 1.1 nm. CoHA/C calcined at 200 °C and reduced at 320 °C are shown in Figs. 8c and 8d, respectively. The spheroid particles of Co_3O_4 (about 16 nm) in the former image converted to inhomogeneously dispersed Co nanoparticles with smaller size (about 12 nm) on reduction at 320 °C.

4. Discussion

The dramatic difference in the behavior of unsupported cobalt(III) hexaammine, and CoHA adsorbed onto silica and carbon is summarized in Fig. 9. Over silica, Co ammines appear to be very stable. Whereas the X-ray absorption methods used here cannot differentiate between O- and N-containing ligands, the XANES and EXAFS data in Figs. 4–7 and Tables 2 and 3 are most easily interpreted as a change in the number of ammine ligands from 6 to 4, whereas Co(III) is reduced to Co(II). This transformation occurs readily (with drying at 100 °C), but then the tetraammine complex appears to be robust through calcination temperatures exceeding 500 °C and reduction temperatures up to 600 °C. The interaction with the silica surface enhances the stability of the Co ammines relative to pure. The strong ad-

Table 4
Co EXAFS fits for $Co(NH_3)_6^{3+}$ on graphite (k^2: $\Delta k = 2.75-12.2^{-1}$ Å)

Catalyst	Treatment	Backscatter	CN	R (Å)	DWF ($\times 10^3$)	E_0 (eV)
CoHA–C	Dried *RT*	Co–O	4.7	1.93	−3.2	−4.4
CoHA–C reduced	Dried *RT*	Co–O	2.2	2.13	1.0	0.1
(CoO + Co)[1]	H_2 at 320 °C	Co–Co	6.6	2.51	1.0	−1.0
		Co–O–Co	5.8	3.02	1.0	−0.5
CoHA–C 100 °C cal	Calcined 100 °C	Co–O	4.8	1.93	−3.2	−4.5
CoHA–C 200 °C cal	Calcined 200 °C	Co–O	5.2	1.94	−3.2	−3.5
CoHA–C 200 °C cal	Calcined 200 °C	Co–O	4.8	1.94	−3.2	−4.3
CoHA–C 200 °C cal reduced	Calcined 200 °C	Co–O	2.7	2.12	1.0	−0.3
(CoO + Co)[2]	Reduced 320 °C	Co–Co	4.8	2.51	1.0	−0.7
		Co–O–Co	8.8	3.02	1.0	0.4

[1] XANES fit: 0.5 Co^{2+} and 0.5 Co^0.
[2] XANES fit: 0.7 Co^{2+} and 0.3 Co^0.

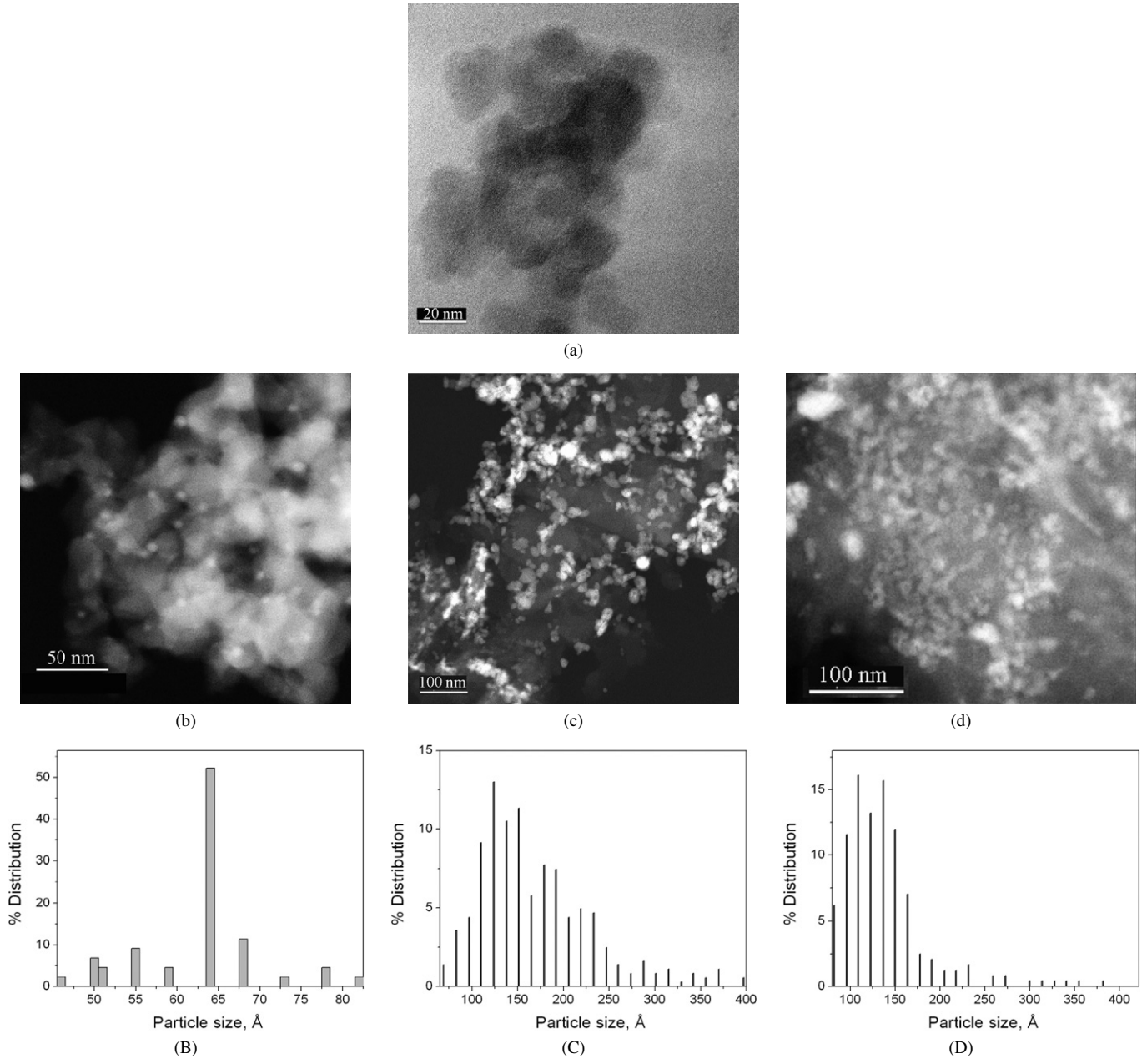

Fig. 8. STEM images of (a) 450 °C calcined 1.8 wt% CoHA/SiO_2, (b) 650 °C reduced 1.8 wt% CoHA/C, (c) 200 °C calcined 5.15 wt% CoHA/C, and (d) 320 °C reduced 5.15 wt% CoHA/C; (B), (C), and (D) are particle size distribution of (b), (c), and (d), respectively.

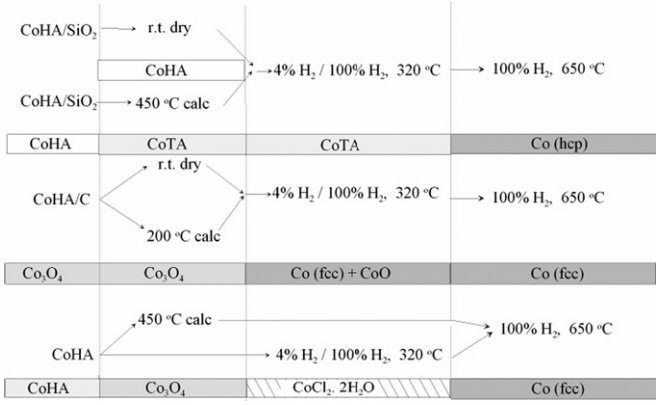

Fig. 9. Schematic of CoHA adsorption on SiO_2 and carbon, calcination and reduction processes. Rectangular box shows chemical state of CoHA in different stages of redox treatments.

sorption of metal ammines complexes on silica gel has been observed for a long time [32–34].

Base metals are known to form phyllosilicate complexes under some preparation conditions [24,35]. The EXAFS spectra of the solution species and the dried precursor (Fig. 4) are essentially the same, and in later stages of pretreatment there are no indications of Co–Co–Si structures in EXAFS data (Figs. 4, 5, and 7) as the Co(III) precursor is reduced to Co(II) and loses 2 ligands. Electron microscopy did not reveal clay-like structures as was recently observed for low-pH preparations of Co/SiO_2 [24]. It may be that the triple-valent Co complex, coordinated with 6 ammine ligands, is more stable to reaction in the aqueous phase than the Co(II) aquoammine intermediates formed in the ammonia method [24]. The formation of phyllosilicates in the Cu/SiO_2 system, which uses a six-coordinate aquoammine complex ($[Cu(NH_3)_4(H_2O)_2]^{2+}$) occurred most readily at the pH (9) corresponding to the maximum of the Cu aquo-hydroxo species ($[Cu(OH)_2(H_2O)_4]^0$), whereas its formation is minimized at higher pH in excess ammonia, where the ammine ligands are stable [35].

Finally, the adsorption density of the Co(III) complex seen in Fig. 1 (1.5 μmol/m^2) is indicative of an adsorbing complex that retains one hydration sheath [1–4]. The retention of hydration sheaths and the adsorption of Pt ammines as outer-sphere complexes over quartz was directly demonstrated in a recent X-ray reflectivity study [36]. The evidence suggests that no physillosilicates form under the conditions used here. It would appear that the adsorption of Co(III) hexaammine complexes over silica under the conditions of this study (i.e., high pH with stable ammine complexes, 1 h of contact) can be adequately described by a purely physical, electrostatic mechanism.

On the other hand, the interaction of CoHA with the graphite surface most definitely has a reactive component. The concurrence of the pH plateaus in Fig. 1A for pure Co_3O_4 and CoHA adsorbed onto silica at 1 h of contact time suggests that the Co ammine has reacted completely to the oxide by this time. Powder XRD of the dried, 1-h contacted sample (Fig. 3IIIc) confirms the formation of cobalt(II, III) oxide from CoHA. Calcination of the dried sample only sinters the Co_3O_4 phase (Fig. 3IIIc). The formation of Co_3O_4 was recently reported over carbon nanofibers with a cobalt carbonate precursor deposited via deposition–precipitation at high pH [22]. In that study, Co^{2+} ammines were observed as intermediate Co species.

The reduction of the Co^{3+} complex to $Co^{2+/3+}$ oxide can be considered a reductive deammination [22] on the carbon surface. Whereas the silica and the carbon substrates used here have the same PZC, the added functionality of semiquinone and pyridine-*N*-oxide groups [37] or the pi bonds in the aromatic rings must give rise to the oxidation–reduction reaction wherein the metal complex is reduced and the carbon surface is oxidized. Carbon has been shown to reduce Pt^{4+} (chloride and oxychloride) complexes to Pt^{2+} at acidic conditions [38,39].

The cobalt oxide formed during CoHA adsorption with carbon is more easily reduced than either the silica-supported ammine precursor or the pure CoHA. Whereas the pure CoHA reduced at 320 °C converts to $CoCl_2{\cdot}2H_2O$, the Co_3O_4 on C converts to CoO and Co metal (Fig. 3) and, at 500 °C, entirely to fcc metal (Fig. 2).

A cited disadvantage of supporting cobalt on silica is that the strong Co precursor–silica interaction leads to a high reduction temperature, at which significant Co sintering occurs [22]. Indeed, we see 6-nm cobalt particles over silica (Fig. 8d, with corresponding Co loading of 1.7 wt%) when the well-dispersed Co ammine precursor (Fig. 8a) is reduced at 650 °C (interestingly, 6–8 nm has been reported to be the optimal Co particle size for Fisher–Tropsch synthesis over Co/CNF [40]). In contrast, Pt ammine precursors strongly adsorbed at pH 10 reduce at 200 °C and form 1-nm particles with 100% dispersion [3]. The reactive interaction of the Co(II) complexes in the ammine method [24] does lead to higher Co dispersions, with particles as small as 3.8 nm at 3 wt% on SiO_2 support. A disadvantage of this method, however, is its complexity; the impregnating solutions must be purged of oxygen to prevent oxidation of the Co, and the preparation must be kept under an inert sweep gas [24]. Higher dispersion of the electrostatically dispersed Co ammine precursor might be achieved with a harsher chemical reduction at lower temperature.

The use of carbon as support for cobalt has been motivated by its potentially weaker interaction with the cobalt complexes, which would allow a lower reduction temperature and minimize sintering [22]. Whereas the reactive deammination of the CoHA complex over carbon may be considered a strong interaction, the product of that interaction is relatively large Co_3O_4 particles, which have less interaction with the carbon surface. Even though these particles become smaller as they are reduced to metal (Fig. 8), as has also been shown for a titania-supported Co_3O_4 precursor phase [41], they are relatively large (average size, about 12 nm). The loading of 3.5 μmol/m^2 (Fig. 1B) at 291 m^2/g, corresponds to a loading of 6.0 wt%. Reduced cobalt particles of 8 nm at 15 wt% Co have been synthesized over carbon nanofibers using HDP [22]. The key to obtaining small carbon supported particles is to find synthesis materials and conditions at which well-dispersed Co oxide or other readily reducible precursor forms; this search is currently ongoing.

There are conflicting reports of the behavior of metallic Co in Co/SiO_2 catalysts in the literature. Sun et al. [42] observed

the fcc phase as the predominant phase in Co/SiO_2 catalyst reduced at 400 °C, while Mishra et al. [43] synthesized nanocomposites of Co/SiO_2 in which Co is in hcp crystal phase, in accordance with pure Co metal phase transition. Another interesting report is that of Lu et al. [44] on Co/SiO_2 core–shell nanoparticles, which found that at a SiO_2 concentration of about 3 mol%, both the hcp and fcc phase exist when reduced at 500 °C, but at a SiO_2 concentration of about 20 mol%, the fcc Co phase and hcp CoO phase exist when reduced at 500 °C for 8 h. When the same material was heated for 16 h, a small amount of hcp Co phase along with fcc Co phase and no CoO phase were seen. These contradictions of different Co phases may be resolved by recent findings of Mattei et al. [45], who studied the size dependence of the hcp-to-fcc transition temperature in Co nanoclusters obtained by ion implantation in silica. They observed a phase-transition temperature of 800 °C for Co/SiO_2 with 5-nm Co particles and concluded that (i) the phase-transition temperature in Co nanoclusters is size-dependent (i.e., increases with decreasing the cluster size) and (ii) the interaction between the matrix and the Co clusters can play a role both in determining the most stable crystalline phase and in controlling the degree of overheating required to achieve hcp-to-fcc transition. They also concluded that kinetic factors can influence the transition.

In the present work, we postulate that the formation of fcc Co phase in Co/C and the hcp Co phase in Co/SiO_2 follows from a combination of size and support effects. Over silica, the CoHA precursor is well dispersed from the strong electrostatic interactions occurring during adsorption. This high initial state of dispersion is maintained to a significant degree through the reduction step; the 6-nm particles are small enough so as to retain their hcp arrangement. But because the CoTA complex is so stable, the reduction is at relatively high temperature, and some sintering does occur relative to the reduction of other metal ammines. The 16-nm Co_3O_4 percursor particles formed over carbon are not small enough to retain the hcp structure and so form fcc.

5. Conclusion

Large differences in adsorptive behavior occur when Co(III) hexaammines are contacted at high pH over silica and carbon surfaces with similar PZCs. The Co ammine–silica interaction can be described by a purely electrostatic interaction, is very strong, and prevents reduction until such high temperatures that significant Co sintering occurs. Sufficient interaction exists that the normally lower-temperature stable hcp phase is retained by the metal crystallites. Higher dispersion over silica might be achieved if the well-dispersed ammine precursor is reduced by a lower-temperature chemical reduction. Over carbon, CoHA undergoes a reduction deammination to form large crystals of Co_3O_4. Whereas this precursor phase reduces at much lower temperature than the silica-supported Co ammines, the large initial size of the Co_3O_4 phase prevents the formation of small Co particles. High Co metal dispersion on carbon might be achieved with synthesis parameters (other Co complexes, carbons, or adsorption conditions) that yield a highly dispersed Co precursor.

Acknowledgment

This work was supported by the National Science Foundation (grant CTS-026051).

References

[1] J.R. Regalbuto, A scientific method to prepare supported catalysts, in: R. Richards (Ed.), Surface and Nanomolecular Catalysis, Taylor & Francis, London, 2006, chap. 6.
[2] J.R. Regalbuto, Preparation of supported metal catalysts by strong electrostatic adsorption (SEA), in: Handbook of Catalyst Preparation, Taylor & Francis, London, 2006, chap. 18.
[3] J.T. Miller, M. Schreier, A.J. Kropf, J.R. Regalbuto, J. Catal. 225 (2004).
[4] J. Regalbuto, Preparation of reforming catalysts, in: Naphtha Reforming, Dekker, New York, 2004, chap. 5.
[5] J.R. Regalbuto, A. Navada, S. Shadid, M.L. Bricker, Q. Chen, J. Catal. 184 (1999) 335.
[6] M. Schreier, J.R. Regalbuto, J. Catal. 225 (2004) 190.
[7] X. Hao, L. Quach, J. Korah, W.A. Spieker, J.R. Regalbuto, J. Mol. Catal. A Chem. 219 (2004) 97.
[8] M. Schreier, S. Teren, L. Belcher, J.R. Regalbuto, J.T. Miller, Nanotechnology 16 (2005) S582.
[9] M.S. Batista, E.I. Santiago, E.M. Assaf, E.A. Ticianelli, J. Power Sources 145 (2005) 50.
[10] M.M. Natile, A. Glisenti, Chem. Mater. 17 (2005) 3403.
[11] J. Mellor, R. Copperthwaite, N. Coville, Appl. Catal. A 164 (1997) 69.
[12] M.S. Batista, R.K.S. Santos, E.M. Assaf, J.M. Assaf, E.A. Ticianelli, J. Power Sources 134 (2004) 27.
[13] W.P. Ma, Y.J. Ding, L.W. Lin, Ind. Eng. Chem. Res. 43 (2004) 2391.
[14] T. Riedel, M. Claeys, H. Schulz, G. Schaub, S.S. Nam, K.W. Jun, M.J. Choi, G. Kishan, K.W. Lee, Appl. Catal. A 186 (1999) 201.
[15] S.V. Gredig, R.A. Koeppel, A. Baiker, Appl. Catal. A 162 (1997) 249.
[16] T. Joh, K. Doyama, K. Fujiwara, K. Maeshima, S. Takahashi, Organometallics 10 (1991) 508.
[17] R.G. Copperthwaite, F.M. Gottschalk, T. Sangiorgio, G.J. Hutchings, Appl. Catal. 63 (1990) L11.
[18] J. Park, J. Kim, L. Hi, Bull. Korean Chem. Soc. 21 (2000) 1239.
[19] G. Hutchings, F. Gottschalk, R. Hunter, S. Orchard, J. Chem. Soc. Faraday Trans. 85 (1989) 363.
[20] T. Halachev, V. Matveev, V. Idakiev, Y. Maksimov, A. Andreev, React. Kinet. Catal. Lett. 32 (1986) 257.
[21] D. Song, J. Li, J. Mol. Catal. A Chem. 247 (2006) 206–212.
[22] G.L. Bezemer, P.B. Radstake, V. Koot, A.J. van Dillen, J.W. Geus, K.P. de Jong, J. Catal. 237 (2006) 291.
[23] H.A. Gasteiger, S.S. Kocha, B. Sompalli, F.T. Wagner, Appl. Catal. B 56 (2005) 9.
[24] A. Barbier, A. Hanif, J.A. Dalmon, G.A. Martin, Appl. Catal. A 168 (1998) 333.
[25] J. Park, J.R. Regalbuto, J. Colloid Interface Sci. 175 (1995) 239.
[26] W.A. Spieker, J. Liu, J.T. Miller, A.J. Kropf, J.R. Regalbuto, Appl. Catal. A 232 (2002) 219.
[27] X. Hao, L. D'Souza, J.R. Regalbuto, Fundamental study of Pt impregnation of carbon 1. Adsorption equilibrium and kinetics, in preparation.
[28] L. D'Souza, J.R. Regalbuto, Preparation of carbon supported cobalt by electrostatic adsorption of Co(III) hexaammines, in preparation.
[29] L.H. Khalil, N.A. Mousssa, S. Mikhail, J. Mater. Sci. 27 (1992) 557.
[30] W.F. Lewis, J. Appl. Phys. 48 (1977) 2980.
[31] J.T. Miller, A.J. Kropf, Y. Zha, J.R. Regalbuto, L. Delannoy, C. Louis, E. Bus, J.A. van Bokhoven, J. Catal. 240 (2006) 222.
[32] G.W. Smith, H.W. Jacobson, J. Phys. Chem. 60 (1956) 1008.
[33] G.W. Smith, L.H. Reyerson, J. Am. Chem. Soc. 52 (1930) 2584.
[34] R. Schwarz, W. Kronig, Chem. Ber. 56B (1923) 208.
[35] T. Toupance, M. Kermarec, J.-F. Lambert, C. Louis, J. Phys. Chem. B 106 (2002) 2277.

[36] C. Park, P. Fenter, N. Sturchio, J. Regalbuto, Phys. Rev. Lett. 94 (2005) 076104/1.
[37] A. Montoya, O.J. Gil, F. Mondragon, N.T. Truong, Fuel Chem. Div. Preprints 47 (2002) 424.
[38] H.E. Van Dam, H. van Bekkum, J. Catal. 131 (1991) 335.
[39] X. Hao, On the Science of Catalyst Preparation: Platinum Impregnation over Carbon, University of Illinois at Chicago, Chicago, 2004.
[40] G.L. Bezemer, J.H. Bitter, H.P.C.E. Kuipers, H. Oosterbeek, J.E. Holewijn, X. Xu, F. Kapteijn, A.J. van Dillen, K.P. de Jong, J. Am. Chem. Soc. 128 (2006) 3956.
[41] F. Morales, D. Grandjean, A. Mens, F.M.F. de Groot, B.M. Weckhuysen, J. Phys. Chem. B 110 (2006) 8626.
[42] S. Sun, N. Tsubaki, K. Fujimoto, J. Chem. Eng. Jpn. 33 (2000) 232.
[43] S.R. Mishra, I. Dubenko, J. Losby, K. Marasinghe, M. Ali, N. Ali, J. Nanosci. Nanotechnol. 5 (2005) 2082.
[44] X. Lu, G. Liang, Z. Sun, W. Zhang, Mater. Sci. Eng. B 117 (2005) 147.
[45] G. Mattei, C. Maurizio, C. de Julian Fernandez, P. Mazzoldi, G. Battaglin, P. Canton, E. Cattaruzza, C. Scian, Nucl. Instrum. Methods Phys. Res. B 250 (2006) 206.
[46] B. Ernst, S. Libs, P. Chaumette, A. Kiennemann, Appl. Catal. A 186 (1999) 145.
[47] K. Okabe, X. Li, M. Wei, H. Arakawa, Catal. Today 89 (2004) 431.
[48] G.L. Bezemer, P.B. Radstake, U. Falke, H. Oosterbeek, H. Kuipers, A. van Dillen, K.P. de Jong, J. Catal. 237 (2006) 152.
[49] R.C. Reuel, C.H. Bartholomew, J. Catal. 85 (1984) 63.